



4-12-2013

## Large-scale Structural Rearrangement of a Serine Hydrolase from *Francisella Tularensis* Facilitates Catalysis

Ekaterina V. Filippova

*Center for Structural Genomics of Infectious Diseases and the Department of Molecular Pharmacology and Biological Chemistry*

Leigh A. Watson

*Butler University*

Misty L. Kuhn

*Center for Structural Genomics of Infectious Diseases and the Department of Molecular Pharmacology and Biological Chemistry*

Brett Geissler

*Northwestern University Feinberg School of Medicine*

Follow this and additional works at: [https://ecommons.luc.edu/chemistry\\_facpubs](https://ecommons.luc.edu/chemistry_facpubs)

Daniel Becker

[daniel.becker@luc.edu](mailto:dbecker3@luc.edu)

### Author Manuscript

This is a pre-publication author manuscript of the final, published article.

### Recommended Citation

Filippova, Ekaterina V.; Watson, Leigh A.; Kuhn, Misty L.; Geissler, Brett; and Becker, Daniel. Large-scale Structural Rearrangement of a Serine Hydrolase from *Francisella Tularensis* Facilitates Catalysis. *Journal of Biological Chemistry*, 288, 15: 10522-10535, 2013. Retrieved from Loyola eCommons, Chemistry: Faculty Publications and Other Works, <http://dx.doi.org/10.1074/jbc.M112.446625>

This Article is brought to you for free and open access by the Faculty Publications and Other Works by Department at Loyola eCommons. It has been accepted for inclusion in Chemistry: Faculty Publications and Other Works by an authorized administrator of Loyola eCommons. For more information, please contact [ecommons@luc.edu](mailto:ecommons@luc.edu).



This work is licensed under a [Creative Commons Attribution-NonCommercial-No Derivative Works 3.0 License](https://creativecommons.org/licenses/by-nc-nd/3.0/).  
© 2013 American Society for Biochemistry and Molecular Biology

Ekaterina V. Filippova<sup>2§</sup>, Leigh A. Weston<sup>1§</sup>, Misty L. Kuhn<sup>2</sup>, Brett Geissler<sup>3</sup>, Alexandra M. Gehring<sup>1</sup>, Nicola Armoush<sup>4</sup>, Chinessa T. Adkins<sup>5</sup>, George Minasov<sup>2</sup>, Ievgeniia Dubrovskaya<sup>2</sup>, Ludmilla Shuvalova<sup>2</sup>, James R. Winsor<sup>2</sup>, Luke D. Lavis<sup>5</sup>, Karla J. F. Satchell<sup>3</sup>, Daniel P. Becker<sup>4</sup>, Wayne F. Anderson<sup>2</sup>, and R. Jeremy Johnson<sup>1\*</sup>

<sup>1</sup>From the Department of Chemistry  
Butler University, Indianapolis, IN 46208.

<sup>2</sup>From the Center for Structural Genomics of Infectious Diseases and the Department of Molecular Pharmacology and Biological Chemistry  
Northwestern University Feinberg School of Medicine, Chicago, IL 60611.

<sup>3</sup>From the Department of Microbiology-Immunology  
Northwestern University Feinberg School of Medicine, Chicago, IL 60611.

<sup>4</sup>From the Department of Chemistry and Biochemistry,  
Loyola University Chicago, Chicago, IL 60660.

<sup>5</sup>HHMI Janelia Farm Research Campus, Ashburn, VA 20147.

\*Running Title: Structural rearrangement of a hydrolase from *F. tularensis*

§Both authors contributed equally to this work

To whom correspondence should be addressed: R. Jeremy Johnson, Department of Chemistry, Butler University, 4600 Sunset Ave, Indianapolis, IN 46208, USA. Tel.: (317) 940-9062; Fax: (317) 940-9519; Email: rjohns1@butler.edu

**Keywords:** serine hydrolases; enzyme structure; protein dynamics; substrate specificity; fluorescence

---

**Background:** Acyl protein thioesterases control protein S-acylation at cellular membranes.

**Results:** FTT258 is a serine hydrolase with broad substrate specificity that binds to bacterial membranes and exists in two distinct conformations.

**Conclusion:** Conformational changes in FTT258 are correlated with catalytic activity.

**Significance:** Structural rearrangement dually regulates the membrane binding and catalytic activity of acyl protein thioesterases.

## SUMMARY

Tularemia is a deadly, febrile disease caused by infection by the gram-negative bacterium, *Francisella tularensis*. Members of the ubiquitous serine hydrolase protein family are amongst current targets to treat diverse bacterial infections. Herein,

we present a structural and functional study of a novel bacterial carboxylesterase (FTT258) from *F. tularensis* - a homologue of human acyl protein thioesterase (hAPT1). The structure of FTT258 has been determined in multiple forms, and unexpectedly large conformational changes of a peripheral flexible loop occur in the presence of a mechanistic cyclobutanone ligand. The concomitant changes in this hydrophobic loop and the newly exposed hydrophobic substrate-binding pocket suggest that the observed structural changes are essential to the biological function and catalytic activity of FTT258. Using diverse substrate libraries, site-directed mutagenesis, and liposome binding assays, we determined the importance of these structural changes to the catalytic activity and membrane binding activity of FTT258. Residues within the newly exposed hydrophobic binding pocket and

**within the peripheral flexible loop proved essential to the hydrolytic activity of FTT258, indicating that structural rearrangement is required for catalytic activity. Both FTT258 and hAPT1 also showed significant association with liposomes designed to mimic bacterial or human membranes, respectively, even though similar structural rearrangements for hAPT1 have not been reported. The necessity for acyl protein thioesterases to have maximal catalytic activity near the membrane surface suggests that these conformational changes in the protein may dually regulate catalytic activity and membrane association in bacterial and human homologues.**

*Francisella tularensis* is an endemic, zoonotic gram-negative bacterium and the causative agent for the febrile disease, tularemia (1,2). While *F. tularensis* infection is uncommon in the general population, the extreme virulence and relatively high mortality rate of *F. tularensis* infection have led to the classification of *F. tularensis*, as a probable biological warfare agent (3,4). As evidence of its extreme virulence, *F. tularensis* infection can be initiated with as few as 10 organisms and if left untreated has mortality rates of 30-60% (5).

Serine hydrolases are an emerging class of therapeutic targets (6-8), including as novel antibiotic targets (9,10). Serine hydrolases (EC: 3.1) are members of the highly conserved  $\alpha/\beta$  hydrolase enzyme superfamily and are involved in a variety of key biological processes in both eukaryotes (neural signaling, signal transduction, and metabolism) and prokaryotes (quorum sensing and virulence) (6,8,11). Evidence of their important biological functions in mammals is shown by the existence of over 110 identified members of this family (6,11). To accomplish their diverse biological roles, serine hydrolases target a variety of compounds that include ester, thioester, and epoxide bonds (12). Members of the superfamily can also catalyze unusual chemical transformations for various commercial applications (12-14). The defining characteristics of this diverse family of enzymes are their conserved  $\alpha/\beta$  hydrolase protein fold, conserved catalytic triad, and conserved catalytic mechanism (12).

One subgroup of serine hydrolases of recent pharmacological interest is eukaryotic acyl protein thioesterases (EC 3.1.2.22), which control

dynamic cycles of S-acylation on a subclass of palmitoylated and membrane-bound proteins (15). The archetype of an acyl protein thioesterase is human acyl protein thioesterase 1 (hAPT1), which controls essential cellular functions including signal transduction, ion transport, and neural development (16-18). hAPT1 was recently confirmed as a target for cancer therapeutics, where inhibition of hAPT1 led to partial phenotypic reversion of Ras-dependent cancers (18). Bacterial lipoproteins are also S-acylated at N-terminal cysteine residues with a growing number of lipoproteins from *F. tularensis* having been directly connected to the virulence and pathogenicity of *F. tularensis* (19-22). These lipoproteins from *F. tularensis* localize to the outer bacterial membrane and activate the mammalian inflammatory response through toll-like receptor 2 (TLR2) signaling (19-22). The central importance of bacterial lipoproteins in the virulence of *F. tularensis* parallels other gram-negative pathogens, including *Neisseria meningitidis*, *Borrelia burgdorferi*, and *Escherichia coli*, where lipoproteins are essential to their infectivity and their recognition by the host immune system (23,24).

Although no bacterial deacylases have been identified, homologues of hAPT1 are found in a variety of bacterial species, including *F. tularensis* (1). Two bacterial homologues of hAPT1 from *Pseudomonas aeruginosa* and *Pseudomonas fluorescens* have been previously characterized as  $\alpha/\beta$  hydrolases with broad substrate specificity and high structural and sequence similarity to hAPT1 (25-27). Despite the important biological functions and potential therapeutic significance of acyl protein thioesterases, structural data is only available for hAPT1 (PDB ID: 1FJ2), PA3859 from *P. aeruginosa* (CPa) (PDB ID: 3CN9 and 3CN7), and carboxylesterase II from *P. fluorescens* (CPf) (PDB ID: 1AUO and 1AUR) (26-28). Each of these enzymes displays a canonical  $\alpha/\beta$  hydrolase fold with a seven-stranded central  $\beta$ -sheet surrounded by six  $\alpha$ -helices and a classic catalytic triad of serine, histidine, and aspartate. Significant variations between the structures were observed in the loop insertions on the edge of the  $\beta$  sheet and in the binding pocket (26-28). These loop insertions in  $\alpha/\beta$  hydrolases often confer their unique substrate specificity or

are responsible for their conformational changes during adsorption to the lipid phase (29). The major difference between the structures of the human and bacterial homologues is that the putative substrate-binding site in hAPT1 is narrower and has limited access compared to the binding pockets of the *Pseudomonas* esterases that can accommodate a range of substrates (26-28). This divergence in structure suggested differential substrate specificities and biological functions between the human and bacterial enzymes (26).

The different conformations of the structures of hAPT1 and bacterial homologues have made comparison of biological functions, catalytic activity, and substrate specificity difficult. Herein, we describe the three-dimensional structure of FTT258, a novel hAPT1 homologue from *F. tularensis*, in two different structural forms and bound to a mechanistic ligand. We determine the catalytic activity and substrate specificity of FTT258 and directly compare this activity to hAPT1. Additionally, we measure the membrane binding ability of FTT258 and hAPT1 and the importance of the conformationally flexible  $\beta_2$  and  $\beta_3$  loops on the catalytic activity of FTT258. Overall, the structural and functional characterization of FTT258 suggests a unique mechanism for linking the regulation of catalytic activity and membrane binding that could control the spatiotemporal activity of acyl protein thioesterases.

## EXPERIMENTAL PROCEDURES

**FTT258 protein preparation and crystallization**—The *FTT258* gene was subcloned into the pMCSG7 vector, heterologously expressed in *E. coli*, and purified as previously described (30). Crystallization trials were conducted using a variety of Qiagen crystallization screens, including Classics II, JCSG+, and PACT. The FTT258 protein (7.4 mg/mL) in 10 mM Tris-HCl pH 8.3 buffer, 500 mM NaCl, 5 mM beta-mercaptoethanol, and 1 mM inhibitor (compound **14**, Figure 1C) was used for the vapor diffusion sitting drop crystallization method with 1  $\mu$ L protein and 1  $\mu$ L reservoir solution. Crystals composed of large plates grew in 0.1M ammonium acetate, 0.1M Bis-Tris pH 5.5, and 17% PEG 10,000 at room temperature after three months. No crystals grew in the absence of cyclobutanone compound.

**Data collection and structure determination**—A single thin plate crystal of FTT258 protein was flash frozen in the reservoir solution. Data were collected at 100 K at the Life Sciences Collaborative Access Team at the Advance Photon Source (Argonne, IL) using a CCD MarMosaic 225 detector. The unit cell was identified with DENZO as P1,  $a = 50.99 \text{ \AA}$ ,  $b = 64.42 \text{ \AA}$ ,  $c = 139.04 \text{ \AA}$ ,  $\alpha = 94.89^\circ$ ,  $\beta = 90.12^\circ$ ,  $\gamma = 89.96^\circ$ . Data were processed with HKL2000 for integration and scaling (31). The structure of FTT258 was solved by molecular replacement with PHASER (32) from the CCP4 suite (33) using the apo-form structure of hAPT1 (PDB ID 1FJ2) as the starting model. Gaps, turns, and side chains for the solved structure were fit manually using the program COOT (34).

**Model refinement and quality of the structure**—In an effort to further improve the map, the free atom refinement procedure and automatic chain tracing as implemented in ARP/wARP were performed (35). Upon completion of model building, the structure was refined by the phenix.refine program (36), using XYZ coordinates, group B-factors, TLS parameters, occupancies and twinning refinement strategies. The automatic recognition of water molecules was resolved in ARP/wARP (35). Details of data collection, structure determination and refinement are provided in Table 1.

The final model of FTT258 consists of eight refined protein molecules (A, B, C, D, E, F, G, H), 459 water molecules and the cyclobutanone ligand **14** covalently bound as the hemiacetal to Ser116 of molecule E. The protein used in this study contains an N-terminal polyhistidine tag (His-tag) plus a Tobacco Etch Virus cleavage site (24 residues long), followed by the FTT258 sequence starting at methionine one. The last two residues of the His-tag are resolved in the electron density map in molecules A, B, C, D and the last three residues of the His-tag in molecules E, F, G, H of the structure. Disordered regions were observed in each of the eight 222 amino acid polypeptide chains in the asymmetric unit, and indicate the localized flexibility of the FTT258 protein structure. The residues that were not well defined include 22-23 and 74-75 in molecules A, B, C, D and additional residues 73, 85, and 104 in molecule A. In molecule E, F, G, and H

disordered regions include residues: 23-25, 53-59, 72-80 from molecule E; 23-25, 53-58, 72-82 from molecule F; 21-26, 51-52, 58-59, 71-79, 91, 149 from molecule G; 22-26, 51-52, 58-62, 71-79 from molecule H. The quality of the model was validated by SFCHECK, PROCHECK, ADIT and MOLPROBITY (37-40) and shows 94% of the residues in the most favored  $\phi/\psi$  regions and no outliers, with the exception of the catalytic residue Ser116 in four molecules (A, D, F, G) of the structure. This unique conformation “a nucleophile elbow” around the catalytic serine has been observed in other  $\alpha/\beta$  hydrolases (41). The atomic coordinates and structure factor data for FTT258 are available from the Protein Data Bank (PDB) with the accession code 4F21.

*Synthesis of cyclobutanone compounds*—Building upon earlier work describing the preparation of variously substituted 2-amino cyclobutanones (42) and an extension of the work by Vederas (43), dimethyl succinate was alkylated (Supplemental Scheme 1) with allyl bromide after deprotonation with LDA to yield dimethyl 2-allylsuccinate **i**, which was then subjected to the general acyloin method of Frahm (44) to afford allyl-substituted (bis-trimethylsilyloxy) cyclobutene **ii**. Treatment of cyclobutene derivative **ii** with *p*-toluenesulfonamide in the presence of HCl afforded allyl-cyclobutanone stereoisomers **iii**, **iv** and **14**, which were separable by normal-phase column chromatography on a gram scale (Supplemental Scheme 1). Regiochemical and stereochemical assignments were made by comparison of DEPT spectra of the three compounds with calculated DEPT spectra generated by SpartanPro'10 (Wavefunction) from *ab initio* density functional level of theory using the RB3LYP functional and the 6-31-G(D) basis sets. Compounds were identified as the ( $\pm$ )-*trans*-3-allyl stereoisomer for the first-eluted isomer **iii**, ( $\pm$ )-*cis*-2-allyl stereoisomer as the second-eluted isomer **iv**, and ( $\pm$ )-*trans*-2-allyl stereoisomer as the third-eluted isomer **14**. A more detailed description of the syntheses and supporting spectral information is included in the Supplemental Material.

*Inhibition assays*—The inhibitory properties of the cyclobutanone compounds on FTT258 were tested using the enzyme purified for crystallization

trials. Activity was measured against *p*-nitrophenyl acetate in the presence or absence of different cyclobutanone compounds (**iii**, **iv**, **14**, Supplemental Scheme 1). The substrate and cyclobutanone compounds were solubilized in 100% ethanol and 100% DMSO, respectively, with 1% final concentration of each solvent in the reaction. The reaction mixture was composed of 100 mM Tris-HCl pH 7.5, 1 mM *p*-nitrophenylacetate, and varying concentrations of cyclobutanone compound in a 0.3 mL volume for 10 min at RT with 23 nM enzyme. The enzyme was incubated with the cyclobutanone compound in buffer for 10 min before starting the reaction. Reactions were initiated with the substrate *p*-nitrophenylacetate, and the initial rate of *p*-nitrophenol production was determined by measuring its absorbance at 415nm in a BioTek ELx808 microplate reader equipped with filters (Biotek Instruments; Winooski, VT). All reactions were performed in triplicate.

*FTT258 purification for kinetic characterization*—A bacterial expression plasmid (pDest17-FTT258) containing the *FTT258* gene from *F. tularensis* (Target GenBank: YP\_169310; protein name FTT258) was obtained from the Harvard Plasmid Repository (Clone ID: FtCD00063611). This bacterial plasmid was transformed into *E. coli* BL21 (DE3) RIPL cells (Agilent). A saturated overnight culture was used to inoculate LB-media (1.0 L) containing ampicillin (100  $\mu$ g/mL) and chloramphenicol (30  $\mu$ g/mL), and the bacterial culture was grown with constant shaking (225 rpm) at 37 °C. Once the OD<sub>600</sub> reached 0.6–0.8, the temperature was dropped to 16 °C and isopropyl  $\beta$ -D-1-thiogalactopyranoside (IPTG; 0.5 mM; Gold Biotechnology) was added to induce protein expression for 12-16 hours. Bacterial cultures were collected by centrifugation at 6,000 x g for 10 min at 4 °C. The bacterial cell pellet was resuspended in PBS (10 mL) and stored at -20 °C.

To disrupt the bacterial cell wall, lysozyme (50 mg; Sigma-Aldrich) and BugBuster detergent (1X, EMD Chemicals) were added and incubated with the cell pellet for 60 min at 25 °C on a rotating shaker. Precipitated proteins and cell material were removed by centrifugation at 18,000 x g for 10 min at 4 °C. Ni-NTA agarose (1 mL; Qiagen) was added to the soluble fraction and incubated at 25 °C for 15 min on a rotating shaker.

The resin was transferred onto a gravity flow column and washed one time each with PBS containing increasing concentrations of imidazole (40 mL each of PBS containing 10 mM imidazole, 25 mM imidazole, or 50 mM imidazole). FTT258 was eluted in PBS containing 250 mM imidazole (600  $\mu$ L) and dialyzed against PBS overnight at 4 °C with constant stirring (10K MWCO; Pierce).

The purity of FTT258 was confirmed by SDS – PAGE on a 4-20% gradient gel and the purity was shown to be greater than 95%. The concentration of FTT258 was determined by measuring the absorbance at 280 nm and by calculating the extinction coefficient ( $\epsilon^{280} = 29910 \text{ M}^{-1} \text{ s}^{-1}$  with all free cysteines) using the modified Edelhoch and Gill/Von Hippel methods on Exspasy (45-47).

*hAPT1 purification*—A bacterial plasmid (pDONR221) containing the *LYPLA1* gene from *Homo sapiens* (Target Genbank: CB008652; protein name hAPT1) was obtained from the Arizona State University Plasmid Repository (Clone ID: HsCD00043610). The *LYPLA1* gene was subcloned into the pDest17 bacterial expression vector using the Gateway cloning system (Invitrogen). The hAPT1 protein was then heterologously expressed in *E. coli* and purified to homogeneity using identical conditions to the purification of FTT258. The concentration of hAPT1 was determined by measuring the absorbance at 280 nm using the extinction coefficient ( $\epsilon^{280} = 20970 \text{ M}^{-1} \text{ s}^{-1}$ ).

*Site-directed mutagenesis and purification*—Variants of FTT258 were created by Quikchange II site-directed mutagenesis using the manufacturer's suggested procedure (Agilent). Proper mutations in the FTT258 DNA sequence were confirmed by DNA sequencing (Genewiz). Plasmids with FTT258 variants were transformed, expressed, and purified using the same procedure as the wild-type FTT258.

*Enzymatic activity against fluorogenic enzyme substrates*—The enzymatic activity of FTT258 was measured against fluorogenic enzyme substrates (Figure 1A) using a 96-well microplate assay (48). Fluorogenic substrates were diluted into PBS containing acetylated BSA (PBS–BSA; 0.1 mg/mL) to a starting concentration of 10  $\mu$ M from 10 mM stock solutions in DMSO. Eight serial dilutions (1:2; 55  $\mu$ L into 165  $\mu$ L total volume) of each substrate (10  $\mu$ M–4.6 nM final

concentrations) were made using PBS–BSA. Fluorogenic enzyme dilutions (95  $\mu$ L) were then transferred to a black 96-well microplate. To initiate the reaction, wild-type or variants of FTT258 (5  $\mu$ L of 125  $\mu$ g/mL) were added to the diluted fluorogenic enzyme substrates in the 96-well microplate. The FTT258 concentration in each reaction was 6.25  $\mu$ g/mL, and the fluorescence change ( $\lambda_{\text{ex}} = 485 \text{ nm}$ ,  $\lambda_{\text{em}} = 528 \text{ nm}$ ) was measured for 4 min at 25 °C on a Biotek Synergy 2 fluorescent plate reader (Biotek Instruments; Winooski, VT). The fluorescence change was converted to molar concentrations using a fluorescein standard curve (30 nM–0.23 nM), which was produced for each experiment. The initial rates of the reactions were measured in triplicate and plotted versus fluorogenic enzyme substrate concentration. The saturation enzyme kinetic traces were fitted to a standard Michaelis–Menten equation and values for  $k_{\text{cat}}$ ,  $K_{\text{M}}$  and  $k_{\text{cat}}/K_{\text{M}}$  were calculated using Origin 6.1 (OriginLab Corp.). The background fluorescence of substrates **1-9** was determined by measuring the kinetics of fluorogenic enzyme substrate hydrolysis using an active site knockout of FTT258 (S116A).

*Enzymatic activity against p-nitrophenyl substrates*—The enzymatic activity of FTT258 was measured against *p*-nitrophenyl acetate, *p*-nitrophenyl butyrate, *p*-nitrophenyl octanoate, and *p*-nitrophenyl laurate (Sigma – Aldrich) (Figure 1B) using a 96-well microplate assay (49). All four substrates, *p*-nitrophenyl acetate (2 M), *p*-nitrophenyl butyrate (2 M), *p*-nitrophenyl octanoate (200 mM), and *p*-nitrophenyl laurate (200 mM) were prepared as stock solutions in acetonitrile and diluted into PBS containing acetylated BSA (PBS–BSA; 0.1 mg/mL) to reduce the nonspecific adsorption to the plasticware common in microplate analysis (50). The starting concentration for *p*-nitrophenyl acetate was 20 mM and for *p*-nitrophenyl butyrate, *p*-nitrophenyl octanoate, and *p*-nitrophenyl laurate was 2 mM. Eight serial dilutions (1:1; 110  $\mu$ L into 220  $\mu$ L total volume; 20 mM–156  $\mu$ M final concentrations for acetate and 2 mM–15.6  $\mu$ M for butyrate, octanoate, and laurate) were made using PBS–BSA containing 1% acetonitrile. Substrate dilutions (95  $\mu$ L) were transferred to a clear 96-well microplate and FTT258 (5  $\mu$ L) was added to start the reaction. FTT258 concentrations in each

reaction were 12.5  $\mu\text{g/mL}$  for acetate and butyrate and 37.5  $\mu\text{g/mL}$  for octanoate and laurate. The absorbance change at 412 nm was measured on a Biotek Synergy 2 fluorescent plate reader for 4 min at 25 °C. The change in absorbance was converted to molar concentrations using the extinction coefficient of *p*-nitrophenol ( $\Delta\varepsilon_{412}=1.034 \text{ mM}^{-1} \text{ cm}^{-1}$ ) (51). Initial rates of the reactions were measured in triplicate and kinetic parameters were determined in the same manner as the fluorogenic assay.

**Liposome binding assay**—Liposomes were prepared with lipids purchased from Avanti Polar Lipids as described previously (52). Bacterial liposomes contained molar ratios of 75% phosphatidylethanolamine, 20% phosphatidylglycerol, and 5% cardiolipin. Eukaryotic liposomes contained molar ratios of 60% phosphatidylcholine, 20% phosphatidylethanolamine, and 20% cholesterol. Purified recombinant proteins (3  $\mu\text{M}$ ) were incubated alone or with liposomes (3 mM) at 37 °C for 5 min then precipitated by ultracentrifugation at  $200,000 \times g$  for 120 min at 25 °C. Proteins in the soluble and pellet fractions were separated by SDS-PAGE and visualized by Coomassie Blue staining.

## RESULTS

**Kinetic characterization of FTT258 and hAPT1**—Acyl protein thioesterases are a highly conserved subclass of serine hydrolases with diverse intracellular substrates and significant therapeutic applications (16). Based on the role of bacterial lipoproteins in the virulence of *F. tularensis* and the confirmed pharmacological importance of hAPT1 (18), we sought to identify and study an APT1 homologue from *F. tularensis* and compare it to hAPT1. The *F. tularensis* subsp. *tularensis* SCHU S4 genome was searched for bacterial homologues to hAPT1 and the gene *FTT258* was identified as a predicted bacterial esterase and potential acyl protein thioesterase. Sequence alignment of the FTT258 protein to diverse APT1 homologues gave high sequence identity to both hAPT1 (39%) and hAPT2 (34%) and to previously characterized bacterial homologues from *P. aeruginosa* (40%) and *P. fluorescens* (38%) (Table 2).

The FTT258 and hAPT1 proteins were heterologously expressed in *E. coli*, purified to

homogeneity, and subjected to detailed kinetic analysis to confirm that FTT258 was a serine hydrolase and compare its activity to previously characterized *Pseudomonas* homologues. Two distinct libraries of esterase substrates were used to determine the enzymatic activity and substrate specificity of the recombinant FTT258 and hAPT1 proteins. The first library consisted of a synthesized set of nine fluorogenic enzyme substrates, which contain ester substituents of varying alkyl length, steric bulk, and stereoelectronic properties (Figure 1A) (53,54). A second esterase library was composed of commercially available *p*-nitrophenyl esterase substrates with acyl ester substituents of various chain lengths (C2, C4, C8, and C12; standard lipid numbering is used where the carbonyl carbon is C1) (Figure 1B). To confirm that FTT258 is a bacterial esterase, the predicted serine nucleophile (Ser116) was mutated to alanine, which ablated all catalytic activity and showed that FTT258 is indeed a classic serine hydrolase with a GxSxG catalytic motif (Table 2) (12,55).

Precise enzyme kinetic measurements of FTT258 and hAPT1 against all nine fluorogenic enzyme substrates produced classic Michaelis-Menten saturation kinetics. The highest catalytic activity of FTT258 was against straight-chain alkyl substrates (substrates 1–5) with maximal activity against valeryl (C5) and butyl (C4) esters (Figure 2A). The catalytic activity increased incrementally from C2 – C5 esters, but then dropped off against the C6 ester (substrate 5). When looking at absolute  $k_{\text{cat}}/K_M$  values, FTT258 maintained catalytic activity greater than  $1.0 \times 10^3 \text{ M}^{-1} \text{ s}^{-1}$  toward all fluorogenic enzyme substrates, except substrates 7 and 8, highlighting the broad substrate specificity of FTT258 toward a wide-range of esters (Supplementary Table 2). Similar broad substrate specificity was observed against *p*-nitrophenyl esters, as FTT258 had  $k_{\text{cat}}/K_M$  values within a factor of two toward alkyl chains ranging from C2 to C8 (Supplementary Table 2). The substrate specificity profile of FTT258 closely parallels the specificity of bacterial homologues from *P. aeruginosa* and *P. fluorescens*, as the *Pseudomonas* homologues also showed broad substrate specificity across a range of shorter alkyl chain (<10 carbons) with maximal activity toward C8 (25-27).

Recombinant hAPT1 and FTT258 had nearly identical relative and absolute  $k_{\text{cat}}/K_M$  values for *p*-nitrophenyl substrates of C4, C8, and C12, (Supplemental Table 2). The enzymatic similarity between FTT258 and hAPT1 does not, however, transfer to the fluorogenic enzyme substrates (Figure 2C). hAPT1 does not display a recognizable trend in catalytic activity toward the library of fluorogenic enzyme substrates (Figure 2C), even toward straight-chain alkyl substrates whereas FTT258 had a nearly linear increase in catalytic activity from C2 – C5 (substrate **1–4**; Figure 2A). The comparison of  $k_{\text{cat}}/K_M$  values between FTT258 and hAPT1 accentuates the broad substrate specificity of FTT258.

*Structure of FTT258*—To determine the level of structural conservation between FTT258 and bacterial and human homologues, crystallization trials were conducted with FTT258. Initial crystallization trials of apo-FTT258 did not yield suitable results, so co-crystallization was conducted in the presence of a cyclobutanone ligand (Figure 1C). Cyclobutanones have previously been explored as reversible  $\beta$ -lactamase inhibitors with modest, but broad-spectrum  $\beta$ -lactamase inhibition. Cyclobutanones also exhibit covalent binding as the hemiketal to the active-site serine of serine hydrolases, as seen crystallographically (56). The three different isomers of a mechanistic cyclobutanone ligand (Supplemental Scheme 1) were screened for relative activity against FTT258 before attempting co-crystallization. Compounds **iii** ( $3.10 \pm 0.12 \mu\text{mol}/\text{min}/\text{mg}$ ), **iv** ( $4.50 \pm 0.08 \mu\text{mol}/\text{min}/\text{mg}$ ), and **14** ( $1.95 \pm 0.21 \mu\text{mol}/\text{min}/\text{mg}$ ) inhibited the catalytic activity of FTT258 ( $4.72 \pm 0.02 \mu\text{mol}/\text{min}/\text{mg}$ ) to varying degrees with compound **14** as the tightest ligand ( $\text{IC}_{50} = 1.12 \text{ mM}$ ). As the ring substituents on the cyclobutanone rings remain consistent, the increased binding affinity for cyclobutanones **iii** and **14** may be due to the conserved *trans* stereochemistry in these two derivatives. Co-crystallization of FTT258 in the presence of the cyclobutanone ligand (**14**) at slightly below its  $\text{IC}_{50}$  value was successful, and the three-dimensional structure was refined to 2.5 Å resolution.

In the final structural model, FTT258 is a monomer but has eight molecules per asymmetric unit. Each molecule shows a canonical  $\alpha/\beta$  hydrolase fold with a classic catalytic triad of

Ser116, His202, and Asp170 (Figures 3A and 4C) and consists of a seven-stranded  $\beta$ -sheet ( $\beta_1$  (2-6),  $\beta_3$  (42-49),  $\beta_2$  (14-21),  $\beta_4$  (109-116),  $\beta_5$  (135-140),  $\beta_6$  (161-168),  $\beta_7$  (191-197)) surrounded by six  $\alpha$ -helices ( $\alpha_1$  (28-36),  $\alpha_2$  (57-65),  $\alpha_3$  (86-103),  $\alpha_4$  (119-127),  $\alpha_5$  (174-187),  $\alpha_6$  (205-220)) and four short helical segments ( $G_1$  (77-80),  $G_2$  (106-109),  $G_3$  (146-149),  $G_4$  (150-153)). The central  $\beta$ -sheet is comprised mostly of parallel strands with the exception of strand  $\beta_1$ , which is antiparallel. The order of the strands within the  $\beta$ -sheet is linear with respect to the sequence except at the N-terminus (Figure 3A), where  $\beta_3$  is positioned between  $\beta_1$  and  $\beta_2$ . The  $\beta$ -sheet lacks the first  $\beta$ -strand of the prototypic  $\alpha/\beta$  hydrolase fold (57).

Among the seven strands in the central  $\beta$  sheet, six parallel  $\beta$  strands,  $\beta_2$ – $\beta_7$ , provide the framework onto which the catalytic residues reside (Figure 3A).

*Large-scale structural rearrangement*—Superposition of the FTT258 subunits within the asymmetric unit reveals two different conformations of the polypeptide chain (Figure 3A). Four molecules of the protein structure (A, B, C and D) show a closed conformation and four molecules (E, F, G, and H) display an open conformation, with one molecule (chain E) covalently bound to a cyclobutanone ligand. The transition between the closed and open forms of FTT258 requires a large conformational change that is centered around the active site and the binding pocket of FTT258 (Figure 3A, 4A, 4B, 4D). The shift between the closed and open forms involves four key changes in the FTT258 structure: 1) reorienting the active site His-Asp dyad, 2) removing the inhibitory action of Asp25, which blocks the substrate binding pocket in the closed form, 3) rearranging the  $\beta_2$  and  $\beta_3$  loops, which exposes the hydrophobic substrate binding pocket, and 4) flipping out a potential membrane binding loop, containing Trp66 and Tyr67. For the ligand bound form, the electron density shows the cyclobutanone moiety of compound **14** covalently bound to Ser116 (Figure 4D), but the remaining substituents on the ligand are unresolved. The lack of strong electron density for the cyclobutanone ligand likely reflects its weak affinity for FTT258.

These large scale rearrangements between the closed and open forms of FTT258 recapitulate

many features of a classic serine hydrolase mechanism where a His-Asp dyad (His202 and Asp170) activates the nucleophilic serine (Ser116) for direct attack on the ester carbonyl (12). In the transition between the closed and open forms of FTT258, the catalytic His-Asp pair shifts with respect to the core of the structure and the nucleophilic serine (Ser116) (Figure 4C). The Ser116 also forms a direct H-bond with the NE2 of His202 in the closed form, which disappears upon rearrangement to the open form (Figure 4D). In the canonical serine hydrolase mechanism, the transient oxyanion formed from the ester carbonyl upon reaction with the catalytic serine is also stabilized by a positively charged oxyanion hole (12). In FTT258, the backbone NH on Leu22 and the NE2 NH of Gln117 form the oxyanion hole in the closed form, and the oxyanion hole becomes occupied by the cyclobutanone hemiacetal oxygen in the ligand bound open state (Figure 4C and 4D). The structural rearrangement also affects the substrate-binding pocket, as Asp25 is positioned across the binding pocket in the closed form occluding the hydrophobic binding pocket. Upon shifting to the open form, the hydrophobic binding pocket is exposed (Figure 4A and 4B), similar to the induced fit binding observed in lipases (29,58).

The conformational rearrangement in the structure of FTT258 also shifts the position of a conserved  $\beta_3$  loop (Figure 3, 4, 5). The movement of the  $\beta_3$  loop is centered around newly exposed tryptophan (Trp66) and tyrosine (Tyr67) residues, which are bracketed by two positively charged residues (Arg64 and Lys70). The exposure of Trp66 and Tyr67 in the FTT258 structure is stabilized by extensive hydrophobic burial of both amino acids in neighboring FTT258 subunits and this interaction is conserved across all subunits in the asymmetric unit (Figure 5). This motif in the  $\beta_3$  loop of hydrophobic residues surrounded by positively charged residues closely match with membrane attachment domains observed in bacterial toxins and predicted in bacterial lipases (52,59). Based on the location, composition, and conservation of residues involved in the conformational change, we hypothesized that the structural rearrangement observed in the crystal structure of FTT258 has direct relevance to its

catalytic activity, substrate specificity, and potentially membrane binding.

*Structural rearrangement in bacterial and human homologues*—To determine if similar structural plasticity was observed in the structures of bacterial and human homologues of FTT258, the open and closed conformations of FTT258 were aligned with the structures of hAPT1, CPa, and CPf. For these structures, the root mean squared difference (RMSD) calculated for the C $\alpha$  atoms between the closed structure of FTT258 and the structures of hAPT1, CPa and CPf are only 1.53 Å, 1.48 Å and 1.45 Å, respectively (Figure 3C). Major differences between the structure of FTT258 and homologous enzymes revolve around the variable movement of the conformationally flexible  $\beta_2$  and  $\beta_3$  loops and proximal  $\beta$ -sheets from the FTT258 structure (Figure 3C).

Interestingly, the closed and open forms of FTT258 more closely mirror the analogous structures from different homologues. The structures of the carboxylesterases from *Pseudomonas* (PDB ID: 3CN9 and 1AUO) displayed an open hydrophobic binding pocket similar to the open form of FTT258, where the  $\beta_2$  and  $\beta_3$  loops are translocated from the binding cavity exposing the large hydrophobic substrate-binding pocket (Figures 3C and 4) (26,27). Similar to the substrate specificities of the *Pseudomonas* homologues, the hydrophobic binding pocket on FTT258 can accommodate a range of hydrophobic substrates using the side chains from putative binding pocket residues Leu22, Leu72, Phe115, and Val172 (26,27). The transition of the  $\beta_2$  and  $\beta_3$  loops in the crystal structure of FTT258 reorients these hydrophobic residues in the active site, suggesting that they play an essential role in binding of FTT258 substrates. Conversely, the closed-form of the FTT258 structure depicts a narrower hydrophobic binding pocket, similar to the hAPT1 structure (Figure 3C) (28). The structural resemblance of the two conformations of FTT258 to the corresponding structural homologues reinforces the hypothesis that the two forms of FTT258 depict snapshots of a structural rearrangement required for catalysis and/or membrane binding. To examine the importance of the structural rearrangement to catalysis and

membrane binding, each of these potential functions was analyzed independently.

*Structural rearrangement and catalytic activity*—To determine the importance of the structural rearrangement to catalytic activity, key residues positioned in the buried hydrophobic binding pocket and in the  $\beta_2$  and  $\beta_3$  loops were substituted with alanine and the kinetic activity of the variants determined against two fluorogenic substrates (substrates **2** and **9**). Amongst amino acids located in the buried hydrophobic binding pocket (Leu22, Leu72, Phe115, and Val172), each one of these hydrophobic residues proved essential for FTT258 catalysis since the enzymatic activity of the alanine variants dropped to near background levels against both substrates **2** and **9** (Figure 2B, Supplemental Table 3). Drastic shifts in enzymatic activity with substitution of each of the binding pocket residues suggests that this hydrophobic network of substrate binding residues is essential to the activity and substrate binding specificity of FTT258. These results also suggest that the exposure of these hydrophobic amino acids upon structural rearrangement is necessary for catalysis, as each of these residues is only accessible in the open conformation (Figure 4). In comparison, a limited sampling of residues located in the hinge regions (Ile57) suggests that hinge residues may not be required for conformational rearrangement, as the Ile57Ala variant retained near wild-type activity. The structural rearrangement is instead likely driven by exposure of  $\beta_3$  loop residues like Trp66 and Tyr67. Reaffirming this hypothesis, substitution of the Trp66 residue alone (W66A) or in concert with Tyr67 (W66A Y67A) nearly ablated catalytic activity with nearly four-orders of magnitude difference in catalytic activity against substrate **2** compared to the wild type FTT258 protein (Figure 2B, Supplemental Table 4). Conversely, Y67A FTT258 showed only a single order of magnitude decrease in activity, indicating that this residue is not critical for catalysis (Figure 2B). Thus, the movement and hydrophobic burial of Trp66 likely controls the structural rearrangement of the substrate-binding pocket observed in FTT258. This structural movement then regulates the catalytic activity of FTT258 by controlling exposure of the substrate-binding pocket and makes structural rearrangement necessary for the full catalytic activity of FTT258.

*Structural rearrangement and membrane binding*—In addition to catalytic activity, the conformational change and exposure of the  $\beta_3$  loop was hypothesized to be directly involved in membrane binding. To test this hypothesis, a liposome-binding assay was used to determine if FTT258 could bind to artificial membranes, where liposome binding was assayed based on the separation of membrane bound and soluble fractions upon centrifugation (Figure 6) (52). The FTT258 protein was prevalent in the pellet fraction when assayed with liposomes designed to mimic bacterial membranes (70% phosphatidylethanolamine, 20% phosphatidylglycerol, and 5% cardiolipin), indicating that FTT258 binds to the bacterial liposomes *in vitro* (Figure 6). The presence of some FTT258 in the soluble fraction suggests that not all of the FTT258 protein was tightly bound to the membrane. Interestingly, the relative percentage of soluble and pellet bound fraction is near 50%, matching with the relative ratio of open and closed conformers in the FTT258 structure (Figure 6). As an important control, FTT258 protein was found almost exclusively in the soluble fraction when liposomes were absent (Figure 6), showing that the presence of the membrane and not the state of protein aggregation determines the fractionation pattern of FTT258. To determine if the Trp66 or Tyr67 residues control membrane association, the single and double alanine substituted variants were tested for liposome binding. Binding of all three FTT258 mutants (W66A, Y67A, or W66A Y67A) to liposomes was indistinguishable from the wild type protein (Figure 6), indicating that other residues on the  $\beta_3$  loop or throughout the protein are more important in membrane binding. Thus, FTT258 is capable of associating with the plasma membrane, but the hydrophobic residues in the conformationally flexible  $\beta_3$  loop do not directly control membrane attachment.

To determine whether the membrane binding observed in FTT258 is conserved in human acyl protein thioesterases, hAPT1 was tested for liposome binding against mammalian specific lipids (Figure 6). hAPT1 showed significant binding to the mammalian membranes, with all of the protein found in the membrane pellet (Figure

6). Thus, although the mechanism of membrane binding is currently unknown, FTT258 and hAPT1 both show similar levels of membrane attachment. The divergence in substrate specificity and catalytic activity between hAPT1 and FTT258 suggests broader cellular substrates and biological functions in FTT258, but similar membrane binding between hAPT1 and FTT258 indicates conserved subcellular localizations for activity.

## DISCUSSION

Serine hydrolases are broadly split into two different subclasses, esterases and lipases, based on substrate specificity and structural characteristics (8,12). Both esterases and lipases have the same active site residues, catalytic mechanism, and overall structural fold ( $\alpha/\beta$  hydrolase fold), but esterases recognize short substrates (< 10 carbons) and lipases hydrolyze ester bonds in longer substrates (> 10 carbons). To maintain substrate specificity for longer carbon substrates, lipases contain an extra structural domain known as a lid that obscures the active site and binding pocket in the closed form, but undergoes large structural rearrangements to expose the hydrophobic binding pocket upon interaction with lipid – water interfaces (29). This interfacial activation at lipid – water boundaries has been proposed to be either thermodynamically driven by the exposure of greater hydrophobic surface at the lipid interface or to be a response to substrate, co-enzyme, or inhibitor binding (29,59).

Based on substrate specificity and the absence of a lid domain, FTT258 is closer to an esterase than a lipase. However, similar to lipases, the structure of FTT258 displayed two distinct conformations based on the large-scale movement of the flexible  $\beta_2$  and  $\beta_3$  loop (Figures 3 and 4). Unlike previous structures of lipase conformations, both forms of FTT258 were present in one asymmetric unit where four subunits (A-D) adopted the closed form and four subunits (E-H) adopted the open form (29,58-60). One subunit of FTT258 also contained electron density for a cyclobutanone ligand that was required for crystallization and was covalently bound to the catalytic serine residue (Figure 4C and 4D). This diversity of structural conformers is rare in protein crystal structures and to the best of

our knowledge, previously unobserved in serine hydrolase structures.

Similar to lid rearrangements in lipases, the structural rearrangement in FTT258 exposes the hydrophobic binding pocket, as Asp25 moves away from the narrow hydrophobic binding pocket. Yet, unlike lipases, the nucleophilic serine and oxyanion hole in FTT258 are solvent exposed prior to loop rearrangement (29,58). Instead, the flexible movement of the  $\beta_2$  and  $\beta_3$  loops on FTT258 mirrors a flexible hydrophobic loop identified on various bacterial lipases, whose movement was independent of lid movement and was proposed to serve as a membrane anchor (59). Similar to this loop on bacterial lipases, the exposed loop on FTT258 is highly hydrophobic, is unlikely to be fully solvent exposed within the cytoplasm, and is highly conserved across FTT258 homologues from mammals to bacteria (Figure 3B and Table 2). In the crystal structure of hAPT1, the  $\beta_3$  loop occupies an identical position to the closed conformation of FTT258 (28), while structures of bacterial homologues from *Pseudomonas* placed the loop closer to the open conformation of FTT258 (26,27). Thus, the conformational flexibility in the  $\beta_2$  and  $\beta_3$  loops is likely conserved across homologues and serves a conserved role in their functions.

The cause of the differential loop shift within the closed and open conformations of FTT258 is unclear. Binding of the cyclobutanone ligand is a potential explanation, but only one of the four subunits of FTT258 crystallized in the open conformation contains a bound cyclobutane ligand. As the cyclobutanone ligand binds only weakly to FTT258 and was present in a concentration (1 mM) around its  $IC_{50}$  value (1.12 mM), the lack of ligand molecules present in the other open conformation subunits might represent the binding and then eventual release of the inhibitors during or after crystallization. Conversely, the different conformations of the loop could reflect the inherent flexibility of the loop, as computational calculations of similar flexible bacterial loops suggested significant movement in aqueous and organic conditions (59). Structures of lipases in open conformations have also been obtained without inhibitors or substrates present (58,60), and the variation in hydrophobic environment has been proposed to stimulate their

interfacial activation through conformational rearrangement of the flexible loops (29,58,59).

The exposure of the hydrophobic  $\beta_2$  and  $\beta_3$  loops in FTT258, and their association with a nearby hydrophobic pocket in a related FTT258 subunit, likely activates FTT258 and represents a biological interaction between the loops and a protein binding partner or cellular membrane.

The connection between structural rearrangement, catalytic activity, and exposure of a potential membrane-binding loop suggests a potential link between the subcellular localization and catalytic activity of FTT258. The structural rearrangement could localize the hydrolase activity of FTT258 near bacterial lipoproteins and serve to control the broad substrate specificity of FTT258. We investigated this hypothesis by examining the role of the structural rearrangement and key residues undergoing conformational change on the catalytic activity and membrane binding of FTT258. The affect of structural arrangement on the catalytic activity originates largely from the emergence of a new hydrophobic binding pocket upon loop rearrangement, as the positioning of the catalytic triad (Ser, His, Asp) remains largely unchanged (Figure 3 and 5). The hydrophobic pocket is lined by a variety of conserved hydrophobic amino acids whose side-chains are indispensable to the enzymatic activity of FTT258 (Figure 2B). Similar to models of Cpa, FTT258 can also accommodate a variety of hydrophobic substrates, especially straight-chain lipid chains of varying lengths (26). The formation of the hydrophobic binding pocket upon structural rearrangement is largely driven by the burial of Trp66 within a nearby subunit of FTT258. The Trp66 residue is required for catalysis (Figure 2B), but is distantly located from the catalytic site in the closed conformation, making direct involvement in the hydrolysis mechanism impossible (Figures 3, 4, and 5). The importance of structural rearrangement for full catalytic activity is reinforced by the essentiality of buried hydrophobic residues to the catalytic activity of FTT258 (Figure 2B), as each of these residues is only fully solvent exposed upon transition to the open form (Figure 4). Thus, the importance of Trp66 to the catalytic activity of FTT258 suggests that structural rearrangement stabilized by burial

of Trp66 serves to control the catalytic activity of FTT258.

Although burial of Trp66 and structural rearrangement is required for full catalytic activity, their role in bacterial membrane binding is less well-defined. FTT258 does localize with bacterial liposomes, but the degree of localization is independent of the presence of Trp66, Tyr67, or both residues combined, making burial of these two hydrophobic amino acids unlikely to control membrane association (Figure 6). Instead, these residues are likely involved in substrate recognition, binding, or interactions with other proteins once FTT258 is bound to the membrane. Further biophysical characterization of FTT258 in the presence of lipid substrates and identification of specific regions of FTT258 responsible for membrane association should clarify the absolute roles of these residues in FTT258 activity.

The membrane association observed for FTT258 is also conserved in the human homologue, hAPT1, where the cellular substrates and cellular compartmentalization are known (15,61). A conserved conformational change for hAPT1 would link the biological role of hAPT1 in recycling proteins such as Ras from the plasma membrane with the cellular location for this role (16). hAPT1 has a conserved tryptophan and a conservatively substituted phenylalanine for tyrosine in its  $\beta_3$  loop (Table 2). hAPT1 and FTT258 however diverged in their substrate specificities, as hAPT1 had significantly decreased enzymatic activity and narrower substrate specificity compared to FTT258, Cpa, and Cpf, especially toward diverse ester substrates (Figure 2). hAPT1 may undergo a similar conformational change to FTT258, but the importance of the structural rearrangement to the catalytic activity of FTT258 and the divergence in activity between FTT258 and hAPT1 will require further investigation.

*Conclusions*—The observed structural rearrangement of the conserved hydrophobic  $\beta_2$  and  $\beta_3$  loops in FTT258 and its affect on catalytic activity and membrane binding provides new hypotheses of how this conserved family of serine hydrolases could potentially control their biological function. Given the confirmed necessity of acyl-protein thioesterases like hAPT1 to depalmitoylate membrane bound proteins (15,18),

the structural rearrangement of FTT258 suggests connected regulation of substrate binding and membrane binding or protein – protein interactions. Whether similar protein acylation cycles exist in bacteria and whether structural rearrangement in acyl-protein thioesterases directly controls acylation remain unanswered questions, but the current study provides a link between substrate binding, structural rearrangement of the active site and hydrophobic

$\beta_2$  and  $\beta_3$  loops, and membrane attachment. With the important biological roles of acyl-protein thioesterases and the validated pharmacological effects of inhibiting hAPT1, the structural rearrangement of FTT258 could provide novel avenues for targeting inhibitors of bacterial and human homologues for the treatment of tularemia and human cancer.

## REFERENCES

1. Beckstrom-Sternberg, S. M., Auerbach, R. K., Godbole, S., Pearson, J. V., Beckstrom-Sternberg, J. S., Deng, Z., Munk, C., Kubota, K., Zhou, Y., Bruce, D., Noronha, J., Scheuermann, R. H., Wang, A., Wei, X., Wang, J., Hao, J., Wagner, D. M., Brettin, T. S., Brown, N., Gilna, P., and Keim, P. S. (2007) Complete genomic characterization of a pathogenic A.II strain of *Francisella tularensis* subspecies tularensis. *PLoS One* **2**, e947
2. McLendon, M. K., Apicella, M. A., and Allen, L. A. (2006) *Francisella tularensis*: taxonomy, genetics, and immunopathogenesis of a potential agent of biowarfare. *Annu. Rev. Microbiol.* **60**, 167-185
3. Pohanka, M., and Skladal, P. (2009) *Bacillus anthracis*, *Francisella tularensis* and *Yersinia pestis*. The most important bacterial warfare agents - review. *Folia Microbiol. (Praha)* **54**, 263-272
4. Oyston, P. C., Sjostedt, A., and Titball, R. W. (2004) Tularaemia: bioterrorism defence renews interest in *Francisella tularensis*. *Nat. Rev. Microbiol.* **2**, 967-978
5. Pechous, R. D., McCarthy, T. R., and Zahrt, T. C. (2009) Working toward the future: insights into *Francisella tularensis* pathogenesis and vaccine development. *Microbiol. Mol. Biol. Rev.* **73**, 684-711
6. Simon, G. M., and Cravatt, B. F. (2010) Activity-based proteomics of enzyme superfamilies: serine hydrolases as a case study. *J. Biol. Chem.* **285**, 11051-11055
7. Bachovchin, D. A., and Cravatt, B. F. (2012) The pharmacological landscape and therapeutic potential of serine hydrolases. *Nat. Rev. Drug Discov.* **11**, 52-68
8. Long, J. Z., and Cravatt, B. F. (2011) The metabolic serine hydrolases and their functions in mammalian physiology and disease. *Chem. Rev.* **111**, 6022-6063
9. West, N. P., Cergol, K. M., Xue, M., Randall, E. J., Britton, W. J., and Payne, R. J. (2011) Inhibitors of an essential mycobacterial cell wall lipase (Rv3802c) as tuberculosis drug leads. *Chem. Commun. (Camb)* **47**, 5166-5168
10. Singh, G., Jadeja, D., and Kaur, J. (2010) Lipid hydrolyzing enzymes in virulence: *Mycobacterium tuberculosis* as a model system. *Crit. Rev. Microbiol.* **36**, 259-269
11. Heal, W. P., and Tate, E. W. (2012) Application of activity-based protein profiling to the study of microbial pathogenesis. *Top. Curr. Chem.* **324**, 115-135
12. Holmquist, M. (2000) Alpha/Beta-hydrolase fold enzymes: structures, functions and mechanisms. *Curr. Protein Pept. Sci.* **1**, 209-235
13. Bornscheuer, U. T. (2002) Microbial carboxyl esterases: classification, properties and application in biocatalysis. *FEMS Microbiol. Rev.* **26**, 73-81
14. Busto, E., Gotor-Fernández, V., and Gotor, V. (2010) Hydrolases: catalytically promiscuous enzymes for non-conventional reactions in organic synthesis. *Chem. Soc. Rev.* **39**, 4504
15. Martin, B. R., Wang, C., Adibekian, A., Tully, S. E., and Cravatt, B. F. (2012) Global profiling of dynamic protein palmitoylation. *Nat. Methods* **9**, 84-89
16. Zeidman, R., Jackson, C. S., and Magee, A. I. (2009) Protein acyl thioesterases (Review). *Mol. Membr. Biol.* **26**, 32-41
17. Siegel, G., Obernosterer, G., Fiore, R., Oehmen, M., Bicker, S., Christensen, M., Khudayberdiev, S., Leuschner, P. F., Busch, C. J., Kane, C., Hubel, K., Dekker, F., Hedberg, C., Rengarajan, B., Drepper, C., Waldmann, H., Kauppinen, S., Greenberg, M. E., Draguhn, A., Rehmsmeier, M., Martinez, J., and Schrott, G. M. (2009) A functional screen implicates microRNA-138-dependent regulation of the depalmitoylation enzyme APT1 in dendritic spine morphogenesis. *Nat. Cell Biol.* **11**, 705-716
18. Dekker, F. J., Rocks, O., Vartak, N., Menninger, S., Hedberg, C., Balamurugan, R., Wetzel, S., Renner, S., Gerauer, M., Scholermann, B., Rusch, M., Kramer, J. W., Rauh, D., Coates, G. W.,

- Brunsveld, L., Bastiaens, P. I., and Waldmann, H. (2010) Small-molecule inhibition of APT1 affects Ras localization and signaling. *Nat. Chem. Biol.* **6**, 449-456
19. Forestal, C. A., Gil, H., Monfett, M., Noah, C. E., Platz, G. J., Thanassi, D. G., Benach, J. L., and Furie, M. B. (2008) A conserved and immunodominant lipoprotein of *Francisella tularensis* is proinflammatory but not essential for virulence. *Microb. Pathog.* **44**, 512-523
  20. Thakran, S., Li, H., Lavine, C. L., Miller, M. A., Bina, J. E., Bina, X. R., and Re, F. (2008) Identification of *Francisella tularensis* lipoproteins that stimulate the toll-like receptor (TLR) 2/TLR1 heterodimer. *J. Biol. Chem.* **283**, 3751-3760
  21. Parra, M. C., Shaffer, S. A., Hajjar, A. M., Gallis, B. M., Hager, A., Goodlett, D. R., Guina, T., Miller, S., and Collins, C. M. (2010) Identification, cloning, expression, and purification of Francisella lpp3: an immunogenic lipoprotein. *Microbiol. Res.* **165**, 531-545
  22. Qin, A., Scott, D. W., Rabideau, M. M., Moore, E. A., and Mann, B. J. (2011) Requirement of the CXXC motif of novel Francisella infectivity potentiator protein B FipB, and FipA in virulence of *F. tularensis subsp. tularensis*. *PLoS One* **6**, e24611
  23. Kovacs-Simon, A., Titball, R. W., and Michell, S. L. (2011) Lipoproteins of bacterial pathogens. *Infect. Immun.* **79**, 548-561
  24. Tokuda, H. (2009) Biogenesis of outer membranes in Gram-negative bacteria. *Biosci. Biotechnol. Biochem.* **73**, 465-473
  25. Pesaresi, A., Devescovi, G., Lamba, D., Venturi, V., and Degrassi, G. (2005) Isolation, characterization, and heterologous expression of a carboxylesterase of *Pseudomonas aeruginosa* PAO1. *Curr. Microbiol.* **50**, 102-109
  26. Pesaresi, A., and Lamba, D. (2010) Insights into the fatty acid chain length specificity of the carboxylesterase PA3859 from *Pseudomonas aeruginosa*: A combined structural, biochemical and computational study. *Biochimie* **92**, 1787-1792
  27. Kim, K. K., Song, H. K., Shin, D. H., Hwang, K. Y., Choe, S., Yoo, O. J., and Suh, S. W. (1997) Crystal structure of carboxylesterase from *Pseudomonas fluorescens*, an alpha/beta hydrolase with broad substrate specificity. *Structure* **5**, 1571-1584
  28. Devedjiev, Y., Dauter, Z., Kuznetsov, S. R., Jones, T. L., and Derewenda, Z. S. (2000) Crystal structure of the human acyl protein thioesterase I from a single X-ray data set to 1.5 Å. *Structure* **8**, 1137-1146
  29. van Tilbeurgh, H., Egloff, M. P., Martinez, C., Rugani, N., Verger, R., and Cambillau, C. (1993) Interfacial activation of the lipase-procolipase complex by mixed micelles revealed by X-ray crystallography. *Nature* **362**, 814-820
  30. Kim, Y., Bigelow, L., Borovilos, M., Dementieva, I., Duggan, E., Eschenfeldt, W., Hatzos, C., Joachimiak, G., Li, H., Maltseva, N., Mulligan, R., Quartey, P., Sather, A., Stols, L., Volkart, L., Wu, R., Zhou, M., and Joachimiak, A. (2008) High-throughput protein purification for x-ray crystallography and NMR. *Adv. Protein Chem. Struct. Biol.* **75**, 85-105
  31. Minor, W., Cymborowski, M., Otwinowski, Z., and Chruszcz, M. (2006) HKL-3000: the integration of data reduction and structure solution--from diffraction images to an initial model in minutes. *Acta Crystallogr. D Biol. Crystallogr.* **62**, 859-866
  32. McCoy, A. J., Grosse-Kunstleve, R. W., Adams, P. D., Winn, M. D., Storoni, L. C., and Read, R. J. (2007) Phaser crystallographic software. *J. Appl. Crystallogr.* **40**, 658-674
  33. Winn, M. D., Ballard, C. C., Cowtan, K. D., Dodson, E. J., Emsley, P., Evans, P. R., Keegan, R. M., Krissinel, E. B., Leslie, A. G., McCoy, A., McNicholas, S. J., Murshudov, G. N., Pannu, N. S., Potterton, E. A., Powell, H. R., Read, R. J., Vagin, A., and Wilson, K. S. (2011) Overview of the CCP4 suite and current developments. *Acta Crystallogr. D Biol. Crystallogr.* **67**, 235-242
  34. Emsley, P., and Cowtan, K. (2004) Coot: model-building tools for molecular graphics. *Acta Crystallogr. D Biol. Crystallogr.* **60**, 2126-2132
  35. Langer, G., Cohen, S. X., Lamzin, V. S., and Perrakis, A. (2008) Automated macromolecular model building for X-ray crystallography using ARP/wARP version 7. *Nat. Protoc.* **3**, 1171-1179

36. Afonine, P. V., Grosse-Kunstleve, R. W., Echols, N., Headd, J. J., Moriarty, N. W., Mustyakimov, M., Terwilliger, T. C., Urzhumtsev, A., Zwart, P. H., and Adams, P. D. (2012) Towards automated crystallographic structure refinement with phenix.refine. *Acta Crystallogr. D Biol. Crystallogr.* **68**, 352-367
37. Vaguine, A. A., Richelle, J., and Wodak, S. J. (1999) SFCHECK: a unified set of procedures for evaluating the quality of macromolecular structure-factor data and their agreement with the atomic model. *Acta Crystallogr. D Biol. Crystallogr.* **55**, 191-205
38. Laskowski, R. A., MacArthur, M. W., Moss, D. S., and Thornton, J. M. (1993) PROCHECK: a program to check the stereochemical quality of protein structures. *J. Appl. Crystallogr.* **26**, 283-291
39. Yang, H., Guranovic, V., Dutta, S., Feng, Z., Berman, H. M., and Westbrook, J. D. (2004) Automated and accurate deposition of structures solved by X-ray diffraction to the Protein Data Bank. *Acta Crystallogr. D Biol. Crystallogr.* **60**, 1833-1839
40. Lovell, S. C., Davis, I. W., Arendall, W. B., 3rd, de Bakker, P. I., Word, J. M., Prisant, M. G., Richardson, J. S., and Richardson, D. C. (2003) Structure validation by C $\alpha$  geometry: phi,psi and C $\beta$  deviation. *Proteins* **50**, 437-450
41. Derewenda, Z. S., and Derewenda, U. (1991) Relationships among serine hydrolases: evidence for a common structural motif in triacylglyceride lipases and esterases. *Biochem. Cell. Biol.* **69**, 842-851
42. Armoush, N., Syal, P., and Becker, D. P. (2008) Synthesis of substituted 2-amino-cyclobutanones. *Synthetic Commun* **38**, 1679-1687
43. Lall, M. S., Ramtohul, Y. K., James, M. N. G., and Vederas, J. C. (2002) Serine and threonine beta-lactones: A new class of hepatitis a virus 3C cysteine proteinase inhibitors. *J Org Chem* **67**, 1536-1547
44. Bisel, P., Breitling, E., and Frahm, A. W. (1998) Diastereo- and Enantioselective Synthesis of (+)- and (-)-cis-2-Aminocyclobutanols. *Eur. J. Org. Chem.* **1998**, 729-733
45. Pace, C. N., Vajdos, F., Fee, L., Grimsley, G., and Gray, T. (1995) How to measure and predict the molar absorption coefficient of a protein. *Protein Sci.* **4**, 2411-2423
46. Edelhoch, H. (1967) Spectroscopic determination of tryptophan and tyrosine in proteins. *Biochemistry* **6**, 1948-1954
47. Gill, S. C., and von Hippel, P. H. (1989) Calculation of protein extinction coefficients from amino acid sequence data. *Anal. Biochem.* **182**, 319-326
48. Lavis, L. D., Chao, T.-Y., and Raines, R. T. (2011) Synthesis and utility of fluorogenic acetoxymethyl ethers. *Chem. Sci.* **2**, 521-530
49. Drzewiecki, K., Angelov, A., Ballschmitz, M., Tiefenbach, K.-J., Sterner, R., and Liebl, W. (2010) Hyperthermostable acetyl xylan esterase. *Microbial biotech.* **3**, 84-92
50. Macarron, R., and Hertzberg, R. P. (2011) Design and implementation of high throughput screening assays. *Mol. Biotechnol.* **47**, 270-285
51. Kim, S., and Lee, S. B. (2004) Thermostable esterase from a thermoacidophilic archaeon: purification and characterization for enzymatic resolution of a chiral compound. *Biosci. Biotechnol. Biochem.* **68**, 2289-2298
52. Geissler, B., Ahrens, S., and Satchell, K. J. (2012) Plasma membrane association of three classes of bacterial toxins is mediated by a basic-hydrophobic motif. *Cell. Microbiol.* **14**, 286-298
53. Tian, L., Yang, Y., Wysocki, L. M., Arnold, A. C., Hu, A., Ravichandran, B., Sternson, S. M., Looger, L. L., and Lavis, L. D. (2012) Selective esterase-ester pair for targeting small molecules with cellular specificity. *Proc. Natl. Acad. Sci. U. S. A.* **109**, 4756-4761
54. Hedge, M. K., Gehring, A. M., Adkins, C. T., Weston, L. A., Lavis, L. D., and Johnson, R. J. (2012) The structural basis for the narrow substrate specificity of an acetyl esterase from *Thermotoga maritima*. *Biochim. Biophys. Acta* **1824**, 1024-1030

55. Kourist, R., Jochens, H., Bartsch, S., Kuipers, R., Padhi, S. K., Gall, M., Bottcher, D., Joosten, H. J., and Bornscheuer, U. T. (2010) The alpha/beta-hydrolase fold 3DM database (ABHDB) as a tool for protein engineering. *ChemBiochem* **11**, 1635-1643
56. Johnson, J. W., Gretes, M., Goodfellow, V. J., Marrone, L., Heynen, M. L., Strynadka, N. C., and Dmitrienko, G. I. (2010) Cyclobutanone analogues of beta-lactams revisited: insights into conformational requirements for inhibition of serine- and metallo-beta-lactamases. *J. Am. Chem. Soc.* **132**, 2558-2560
57. Ollis, D. L., Cheah, E., Cygler, M., Dijkstra, B., Frolow, F., Franken, S. M., Harel, M., Remington, S. J., Silman, I., Schrag, J., and et al. (1992) The alpha/beta hydrolase fold. *Protein Eng.* **5**, 197-211
58. Schrag, J. D., Li, Y., Cygler, M., Lang, D., Burgdorf, T., Hecht, H. J., Schmid, R., Schomburg, D., Rydel, T. J., Oliver, J. D., Strickland, L. C., Dunaway, C. M., Larson, S. B., Day, J., and McPherson, A. (1997) The open conformation of a *Pseudomonas* lipase. *Structure* **5**, 187-202
59. Rehm, S., Trodler, P., and Pleiss, J. (2010) Solvent-induced lid opening in lipases: a molecular dynamics study. *Protein Sci.* **19**, 2122-2130
60. Kim, K. K., Song, H. K., Shin, D. H., Hwang, K. Y., and Suh, S. W. (1997) The crystal structure of a triacylglycerol lipase from *Pseudomonas cepacia* reveals a highly open conformation in the absence of a bound inhibitor. *Structure* **5**, 173-185
61. Hirano, T., Kishi, M., Sugimoto, H., Taguchi, R., Obinata, H., Ohshima, N., Tatei, K., and Izumi, T. (2009) Thioesterase activity and subcellular localization of acylprotein thioesterase 1/lysophospholipase 1. *Biochim. Biophys. Acta* **1791**, 797-805
62. Chenna, R., Sugawara, H., Koike, T., Lopez, R., Gibson, T. J., Higgins, D. G., and Thompson, J. D. (2003) Multiple sequence alignment with the Clustal series of programs. *Nucleic Acids Res.* **31**, 3497-3500

*Acknowledgments*—We thank Matthew Hedge and Geoffrey Hoops for contributive discussions.

## FOOTNOTES

\*This project has been funded in whole or in part with Federal funds from the National Institute of Allergy and Infectious Diseases, National Institutes of Health, Department of Health and Human Services, under Contract No. HHSN272200700058C (to W.F.A.). L.A.W. and A.M.G. were supported by a Holcomb grant from Butler University. R.J.J. was supported by start-up funds and a Holcomb grant from Butler University and a Senior Research Grant from the Indiana Academy of Sciences. C.T.A. and L.D.L. were supported by the Howard Hughes Medical Institute. A portion of this work was supported by NIH award AI051490 (to K.J.F.S) and an Investigator in the Pathogenesis of Infectious Disease award from the Burroughs Wellcome Fund (to K.J.F.S.).

<sup>§</sup>Both authors contributed equally to this work

<sup>1</sup>To whom correspondence should be addressed: R. Jeremy Johnson, Department of Chemistry, Butler University, 4600 Sunset Ave, Indianapolis, IN 46208, USA. Tel.: (317) 940-9062; Fax: (317) 940-9519; Email: rjohns1@butler.edu

<sup>2</sup>Center for Structural Genomics of Infectious Diseases, Northwestern Feinberg School of Medicine, Department of Molecular Pharmacology and Biological Chemistry, 303 E. Chicago Ave., Chicago, IL 60611.

<sup>3</sup>Northwestern University Feinberg School of Medicine, Department of Microbiology-Immunology, 303 E. Chicago Ave., Chicago, IL 60611.

<sup>4</sup>Loyola University Chicago, Department of Chemistry & Biochemistry, 1032 W. Sheridan Rd., Chicago, IL 60660.

<sup>5</sup>HHMI Janelia Farm Research Campus, 19700 Helix Dr, Ashburn, VA 20147.

<sup>6</sup>The abbreviations used are: Cpa; bacterial carboxylesterase PA3859 from *Pseudomonas aeruginosa*; Cpf, bacterial carboxylesterase II from *Pseudomonas fluorescens*; FTT258, bacterial carboxylesterase from *Francisella tularensis*; hAPT1; human acyl protein thioesterase 1; His-tag, N-terminal polyhistidine tag; IPTG, isopropyl  $\beta$ -D-1-thiogalactopyranoside; MWCO, molecular weight cut-off; PDB, protein data bank; RMSD, root mean square deviation; TLR2, toll-like receptor 2

## FIGURE LEGENDS

**FIGURE 1.** FTT258 substrates and ligand. *A*, Fluorogenic hydrolase substrates. All substrates contain a fluorescein moiety and two acyloxymethyl ether substituents with varied R-groups. The functional groups on the nine fluorogenic enzyme substrates were designed to measure the ability of FTT258 to adapt to slight differences in carbon chain length (substrates **1-5**), to accommodate steric bulk and changes in electronic structure (substrates **6** and **7**), and to hydrolyze substrates bearing quaternary carbons alpha to the ester carbonyl (substrates **8** and **9**). *B*, Nitrophenyl hydrolase substrates. Substrates represent different carbon chain lengths: *p*-nitrophenyl acetate (substrate **10**, C2), *p*-nitrophenyl butyrate (substrate **11**, C4), *p*-nitrophenyl octanoate (substrate **12**, C8), and *p*-nitrophenyl laurate (substrate **13**, C12). *C*, Mechanistic cyclobutanone ligand. Compound **14** (( $\pm$ )-*trans*-2-allyl)) was synthesized as described in supplemental methods and was co-crystallized bound to the serine nucleophile of FTT258.

**FIGURE 2.** Enzymatic characterization and substrate specificity of FTT258 and hAPT1. *A*, Substrate specificity of FTT258. Enzymatic efficiency of fluorogenic substrate hydrolysis by FTT258 against all nine members of the substrate library (Figure 1A). Kinetic values are given in Supplemental Table 2. *B*, Substrate specificity of hAPT1. Enzymatic efficiency of fluorogenic enzyme substrate hydrolysis by hAPT1 against all nine members of the substrate library (Figure 1A). Kinetic values are given in Supplemental Table 2. *C*, Comparison of the enzymatic efficiency ( $k_{cat}/K_m$ ) of FTT258 variants against substrates **2** and **9**. All enzymatic efficiency values for FTT258 variants were normalized based on the

enzymatic efficiency of wild-type FTT258 against each substrate (Supplemental Table 2). Kinetic values for each FTT258 variant and substrate are given in Supplemental Table 3.

**FIGURE 3.** Structure of FTT258 and comparison to homologues. *A*, Comparison of an FTT258 monomer in the closed form (coral) and in the open form (green) in complex with inhibitor (**14**) (ball-and-stick model colored in tan). Secondary structure elements are labeled. The catalytic residues (Ser116, His202, and Asp170) are shown as sticks and colored by atom type (oxygen in red, carbon in yellow, nitrogen in blue). *B*, Surface representation of the FTT258 molecule colored according to sequence conservation [from dark blue (highly variable) to red (invariant)]. *C*, Stereo view of the closed (coral) and open (green) forms of the FTT258 monomer superimposed onto the monomeric structures of hAPT1 (blue), CPa (purple) and CPf (yellow). Termini of secondary structural elements on FTT258 are labeled. Conserved Trp66 and Tyr67 residues localized on the  $\beta_3$  loop are shown as stick models and colored by the FTT258 molecule type.

**FIGURE 4.** Electrostatic surface of the binding pocket in FTT258. *A* and *B*, Electrostatic surface representation of the putative binding pocket in closed (*A*) and open (*B*) form of the FTT258 structure. Compound **14** bound in the active site is shown as sticks (red). Conserved residues surrounding the active site are labeled in the structures. Hydrophobic residues substituted with alanine in FTT258 protein are colored in blue. Negative (red), positive (blue), and neutral (white) charged regions on the molecules surface are colored. *C*, Binding pocket residues in the open inhibitor-bound form of FTT258. Compound **14** is shown as a ball and stick coral model in the electron density ( $2F_o - F_c$ ) map contoured at  $1\sigma$ . The model is colored by atom type (oxygen in red, carbon in green, nitrogen in blue). *D*, Superposition of closed (coral) and open inhibitor-bound (green) active sites.

**FIGURE 5.** Contact interface between residues of the  $\beta_3$  loop with neighboring molecules in the crystal lattice. *A*, In the model, oxygen atoms of the residues are colored in red, nitrogen in blue, sulfur in yellow, and carbon in coral. Negative (red) and neutral (white) charged regions on the electrostatic surface are also colored. *B*, Contact interface between residues of the  $\beta_3$  loop in the closed form (coral) and open form (green) with neighboring molecules in the crystal lattice (light blue and purple, respectively).

**FIGURE 6.** FTT258 and hAPT1 associate with liposomes. *A*, The indicated proteins (3  $\mu$ M) were incubated with 3 mM bacterial (FTT258) or eukaryotic (hAPT1) liposomes (lipos +) or in buffer alone (lipos -) at 37 °C for 5 min and separated by ultracentrifugation. The proteins in the soluble (S) and pellet (P) fractions were then separated by SDS-PAGE and visualized by Coomassie Blue staining. *B*, The indicated  $\beta_3$ -loop variants of FTT258 were incubated with bacterial liposomes (+ lipos) or in buffer alone (- lipos) and separated by ultracentrifugation and visualization as in *A*. Representative gels from at least two separate experiments are shown. WA-YA indicates the double mutation W67A and Y68A.

Table 1. Crystallographic parameters, data-collection and refinement statistics. Data for the highest resolution shell are given in parentheses.

<b>Data collection</b>	
Resolution (Å)	30.0-2.5 (2.54-2.50)
Completeness (%)	94.4 (97.5)
Observed/unique reflections	108535/58087
Redundancy	1.9 (1.8)
I/s(I)	8.4 (2.2)
R <sub>merge</sub> (%)	7.8 (36)
Wilson B-factor (Å <sup>2</sup> )	47.20
<b>Refinement</b>	
R (%) / R <sub>free</sub> (%)	19.9/25.8
R.m.s. deviations from idealized geometry:	0.003
Bond lengths (Å)	0.8
Bond angles (°)	
Mean B value (Å <sup>2</sup> ):	46.47
Main chain atoms	46.50
Side chain atoms	26.85
Waters	32.88
Heteroatoms (inhibitor)	
Total number of non-hydrogen atoms:	13268
Protein atoms	459
Water molecules	

Table 2: Sequence alignment of amino acids in the FTT258 active site, binding pocket, and membrane binding loop.

Organism	22	57	66-67	72	115	114-120	170	172	202	% Identity
<i>F. tularensis</i>	L	I	WY	L	F	GFSQGG	D	V	H	-
<i>F. philomiragia</i>	L	I	WY	L	F	GFSQGG	D	V	H	90
<i>M. aquaeolei</i>	L	I	WY	M	F	GFSQGG	D	I	H	42
<i>S. denitrificans</i>	L	I	WY	L	F	GFSQGG	D	V	H	41
<i>B. taurus</i> (1)	L	L	WF	L	F	GFSQGG	D	L	H	40
<i>P. aeruginosa</i>	L	V	WY	F	F	GFSQGG	D	V	H	40
<i>H. sapiens</i> (1)	L	L	WF	L	F	GFSQGG	D	L	H	39
<i>P. fluorescens</i>	L	I	WY	M	F	GFSQGG	D	V	H	38
<i>H. sapiens</i> (2)	L	L	WF	L	F	GFSQGG	D	M	H	34

<sup>a</sup>The amino acid sequence of FTT258 was aligned using ClustalW (62). The amino acid numbering corresponds to the amino acid numbering in FTT258. The number in parentheses refers to whether the protein has been designated as a closer homologue of human APT1 (1) or APT2 (2). The sequences used in the alignment were from *F. tularensis* (NCBI Ref Seq: YP\_169310.1), *Francisella philomiragia* (NCBI Ref Seq: YP\_001677414.1), *Marinobacter aquaeolei* (NCBI Ref Seq: YP\_960546.1), *Shewanella denitrificans* (NCBI Ref Seq: YP\_563143.1), *Bos taurus* (UniprotKB: Q3MHR0), *P. aeruginosa* (NCBI Ref Seq: NP\_252548.1), *Homo sapiens* (APT1 UniprotKB: O75608; APT2 UniprotKB: O95372), *P. fluorescens* (UniprotKB: Q51758). For full alignment, see Supplemental Figure 1.

Figure 1

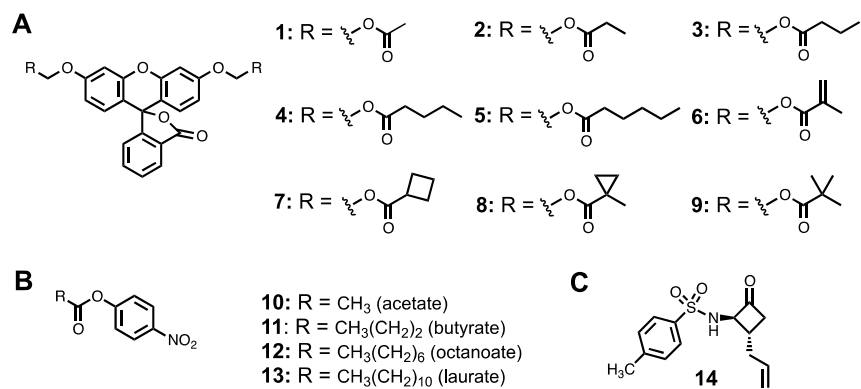


Figure 2

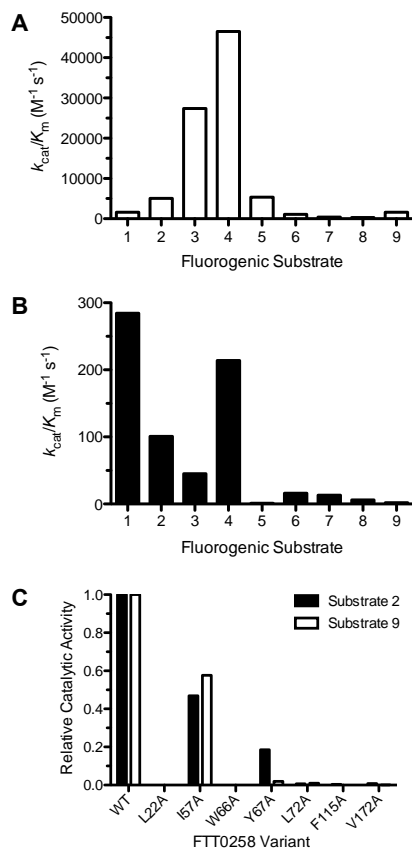


Figure 3

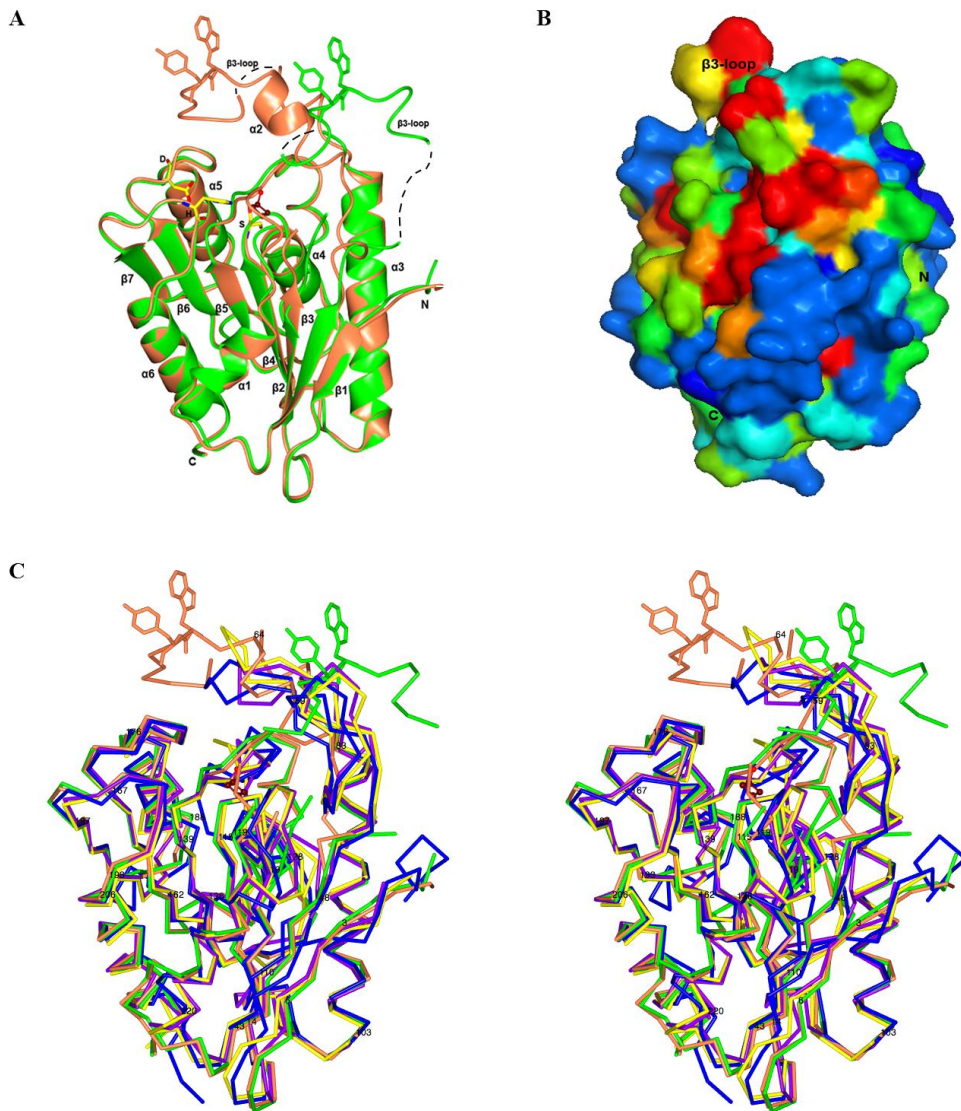


Figure 4

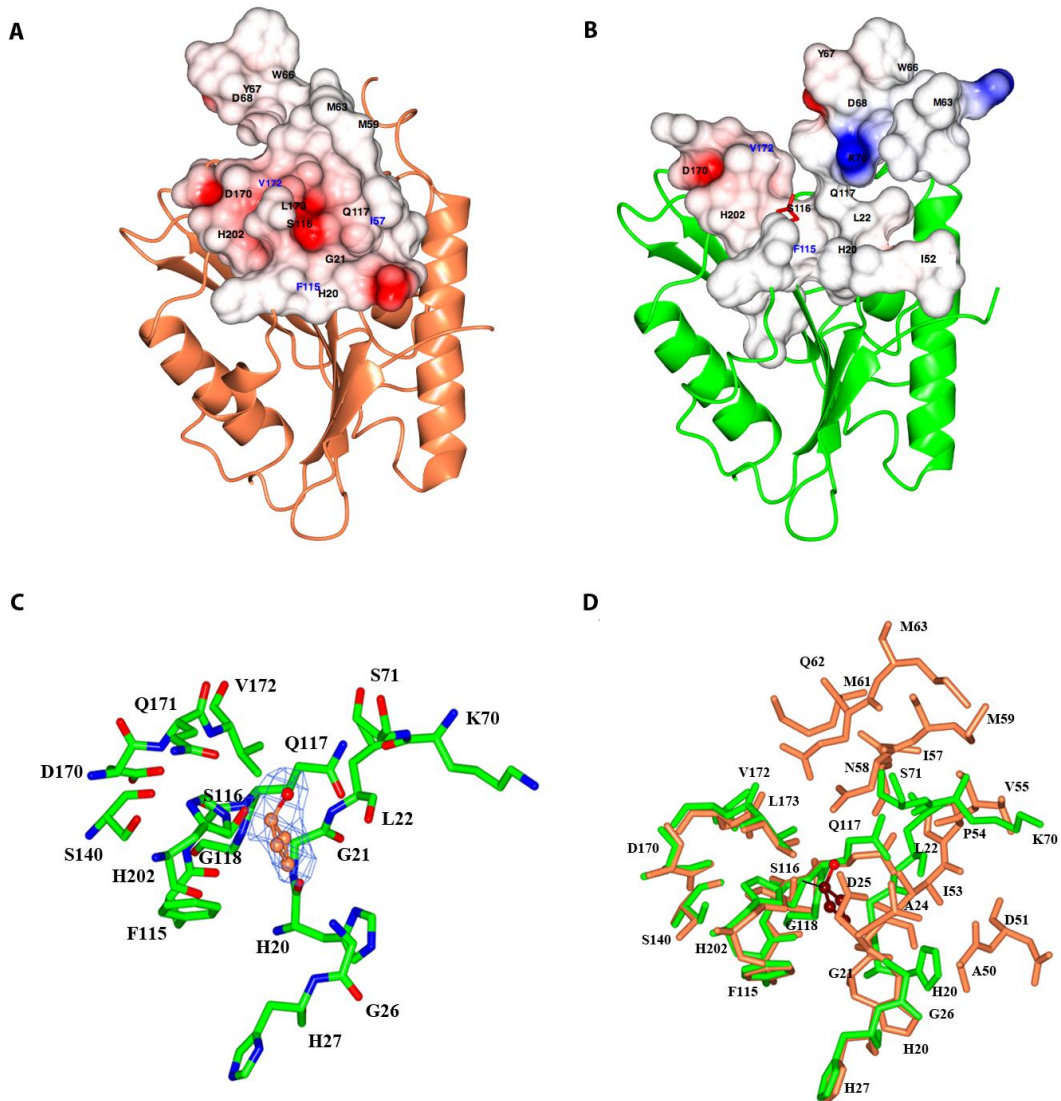


Figure 5

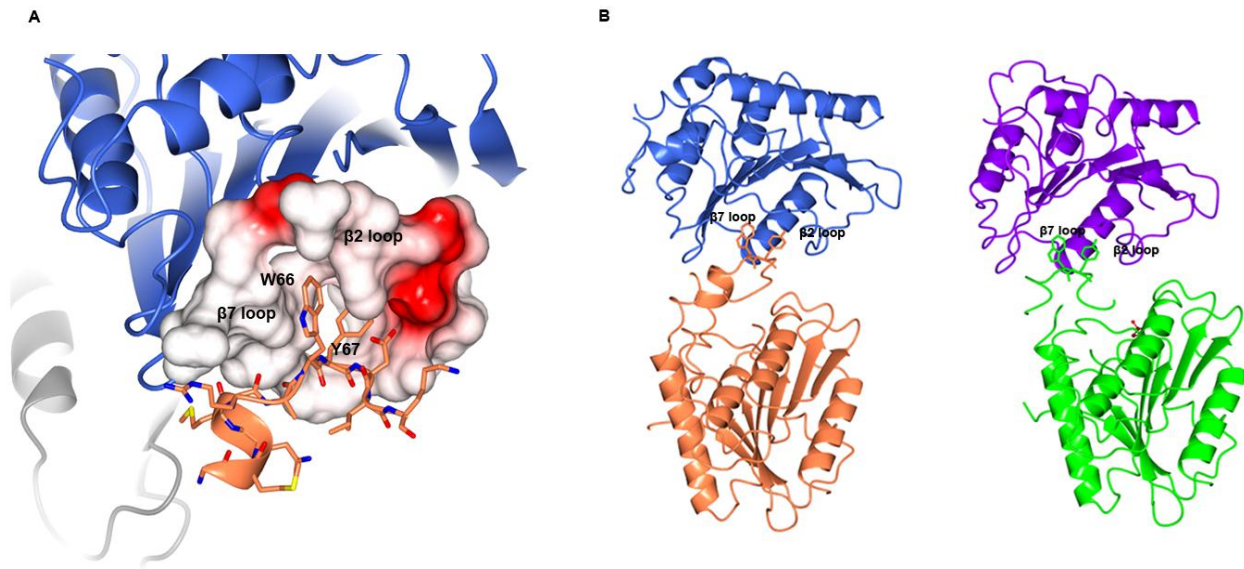


Figure 6

